ORIGINAL ARTICLE – RESEARCH

WILEY

Comparison between optical coherence tomographic and histopathologic appearances of artifacts caused by common surgical conditions and instrumentation

Christina J. Cocca DVM[1] | Laura E. Selmic BVetMed (Hons), MPH, DACVS-SA[1] |
Jonathan Samuelson DVM, DACVP[2] | Pin-Chieh Huang MS[3,4] | Jianfeng Wang PhD[3] |
Stephen A. Boppart MD, PhD[3,4,5,6]

[1]Department of Veterinary Clinical Medicine, University of Illinois Urbana-Champaign, Urbana, Illinois

[2]Department of Pathobiology, University of Illinois Urbana-Champaign, Urbana, Illinois

[3]Beckman Institute for Advanced Science and Technology, University of Illinois Urbana-Champaign, Urbana, Illinois

[4]Department of Bioengineering, University of Illinois Urbana-Champaign, Urbana, Illinois

[5]Department of Electrical and Computer Engineering, University of Illinois Urbana-Champaign, Urbana, Illinois

[6]Carle-Illinois College of Medicine, University of Illinois Urbana-Champaign, Urbana, Illinois

Correspondence
Laura E. Selmic, The Ohio State University Veterinary Teaching Hospital, 601 Vernon L. Tharp St, Columbus, OH 43210.
Email: selmic.1@osu.edu

Abstract

Objective: To document the appearance of artifacts created by commonly encountered surgical conditions and instrumentation on optical coherence tomography (OCT) and to compare these findings with histopathology.

Study design: Ex vivo study.

Animals: Five canine cadavers.

Methods: Skin, subcutaneous fat, skeletal muscle, and fascia samples were obtained from fresh canine cadavers. Blood pooling, hemostatic crushing, scalpel blade cut, monopolar electrosurgery, bipolar vessel sealing device, and ultrasonic energy surgical artifacts were induced on each tissue type. Each specimen was imaged with OCT and subsequently histologically processed.

Results: Most surgical instrumentation used for tumor excision created a high-scattering region with local architectural disruption. Blood pooling was visible as a high-scattering layer overlying tissue with normal architecture. Only the scalpel blade created a focal, low-scattering area representing a sharply demarcated cut within the tissue distinct from the appearance of other instrumentation.

Conclusion: Common surgical instruments and conditions encountered during tumor excision produced high-scattering OCT artifacts in tissues commonly seen at surgical margins.

Clinical significance: The clinical value of OCT hinges on the ability of personnel to interpret this novel imaging and recognize artifacts. Defining and describing the appearance of common surgical artifacts provides a foundation to create image libraries with known histological and OCT interpretation, ultimately improving the diagnostic accuracy of OCT for assessment of surgical margins.

1 | INTRODUCTION

Cancer is one of the leading causes of death in companion animals and comes with a high cost to owners, both financially and emotionally. Tumors are often surgically excised

with a varying amount of normal surrounding tissue deemed the surgical margin. A complete surgical margin is defined as the absence of neoplastic cells at the inked margin, suggesting that all of the neoplastic tissue has been removed.[1] Surgical removal of tumors with complete margins decreases local recurrence and increases disease free interval, overall survival time, and the time to recurrence or metastasis.[2,3] Therefore, the ability to evaluate surgical margins to determine the extent of tumor resection in real time is of critical value.

Margin assessment in veterinary medicine has historically focused on histopathological evaluation of the ex vivo surgical specimen, requiring days for routine processing. Various intraoperative techniques have been developed and evaluated for their ability to provide information about the neoplastic potential of surgical margins or the resection bed within a time frame that allows for intervention at the time of the initial surgery.[4] Established intraoperative techniques include frozen section analysis, touch preparation (imprint) cytology, and intraoperative ultrasound.[4] However, limitations such as increased operative times, distortion between correlation of the tumor and tumor bed, and the limited ability of sampling have spurred the growing interest in the development of novel microscopic optical imaging techniques.[5] Near-infrared fluorescence imaging has been developed and refined in the last decade as an optical modality to allow for real-time, intraoperative assessment of tumor margins during cancer surgery. Cabon et al[6] used canine models to evaluate the use of intraoperative fluorescence imaging in the resection of malignant masses using a novel nanoparticle contrast agent. Results from their study provided evidence of tumor fluorescence in all spontaneously occurring tumors and good correlation between the presence of residual tumor bed fluorescence and histopathology.

Optical coherence tomography (OCT) is a noninvasive optical imaging technique that provides high-resolution, cross-sectional optical images of microscopic tissue structure in real time with the use of near-infrared light waves.[7-11] Tissues then reflect light waves back, and each scanning point is interpreted as a depth profile on the basis of the density of cells. The images generated are similar in appearance to ultrasound, with a much higher resolution (<20 μm) and a shallower imaging depth (1–2 mm). Optical coherence tomography is a powerful imaging technique that can detect morphological changes at the cellular level without compromising the integrity and viability of surgical margins.

Optical coherence tomography has been previously used in human breast cancer research to image surgical margins for differentiation between normal and cancerous tissue. The goal of using OCT in human breast cancer lumpectomy is to facilitate removal of the smallest possible amount of normal tissue while ensuring that the tumor tissue is completely excised. Optical coherence tomography has the ability to increase intraoperative detection of residual disease to ensure good local control while eliminating the requirement for future reintervention. The reported sensitivity and specificity of OCT to identify positive margins is 100% and 82%, respectively.[7]

The veterinary literature contains little information regarding the use of OCT in identifying the presence of neoplastic cells in surgical margins. Optical coherence tomography has been used only as a guidance tool for the intraoperative assessment of soft tissue sarcoma margins[12] and to help guide the pathologic interrogation of excised mast cell and anal sac tumors.[13] In addition, the appearance of common surgical artifacts that could occur during tumor resection has not been evaluated.

The objective of this study was to document the appearance of artifacts created by commonly encountered surgical conditions and instrumentation on OCT and to compare these findings with histopathology. We hypothesized that a cutting defect would appear as a void or area of low-scattering intensity, whereas the use of various forms of electrosurgery equipment would cause dissemination of energy in the form of heat, resulting in prominent areas of adjacent high optical scattering. Characterization of these surgical artifacts are crucial to help OCT observers distinguish between native and artifactual tissue alteration, enhancing the accuracy of tumor resection.

2 | MATERIALS AND METHODS

2.1 | Specimen preparation

The use of cadavers was approved by the Institutional Animal Care and Use Committee at the University of Illinois. Five canine cadavers were acquired and used no more than 6 hours after being humanely euthanized for reasons unrelated to the present study. The number of cadavers employed was based on preclinical research in which a similar protocol was used. The dogs had no known history of dermatological or systemic disease that would alter gross tissue morphology.

The hair overlying the dorsal epaxial and lateral abdomen was clipped in preparation for specimen acquisition. A 16- × 4-cm area of tissue overlying the lateral abdomen and dorsal epaxial region was identified. A grid was drawn on the tissue with a surgical marker creating two trials (each with eight surgical artifacts) of eight, 2- × 2-cm boxes, to minimize variability within results of each tissue sample. The lateral abdomen was used to harvest skin and subcutaneous fat, while the dorsal epaxial region was used for fascia and skeletal muscle samples. These regions were chosen because they offered a large area of homogenous tissue sampling and maximized the utility of each canine cadaver. Sixteen specimens were created from each of the predetermined tissue types (skin, subcutaneous fat, fascia, skeletal muscle), creating a total of 64 tissue specimens for each canine cadaver.

2.2 | Surgical artifact creation

The following surgical artifacts were created on each 2- × 2-cm tissue sample in a consecutive manner: blood pooling, hemostatic crushing, full thickness No. 10 scalpel blade cut, monopolar electrosurgery applied in cutting function at three increasing energy settings (5, 15, 25 W), bipolar vessel sealing device (LigaSure Atlas), and ultrasonic energy (harmonic scalpel) applied on a maximum setting. Blood pooling artifacts were created by placing 1 to 2 mL of autologous fresh whole blood on the tissue surface just prior to image acquisition. Crushing artifacts were created with a Mosquito hemostat, with the ratchet tightened to its maximal extent. Monopolar electrosurgery settings were based on what was most commonly used in a clinical setting during tumor resection. The LigaSure Atlas handpiece was used to create all bipolar vessel sealing device artifacts, and the harmonic scalpel hook blade was used for the respective ultrasonic energy artifacts. All surgical artifacts were created by a single surgical resident (C.J.C.) under the supervision of an American College of Veterinary Surgeons diplomate.

2.3 | Optical coherence tomographic imaging

After artifact creation, each specimen was imaged in situ with a clinical spectral-domain OCT system (University of Illinois; Figure 1). Optical coherence tomography of the specimen in B-mode was performed in a systematic fashion allowing for continuous scanning across the affected area of tissue in addition to static imaging wherever abnormalities were identified. The imaging pattern was recorded and used to orient subsequent histopathology sections. Optical coherence tomographic images were evaluated by one of the investigators of the study at the time of acquisition to ensure images were of sufficient quality for evaluation.

2.4 | Histopathological evaluation

Each tissue specimen was excised and placed in 10% neutral buffered formalin at a 1:10 ratio in a plastic container of appropriate size within 30 minutes from the time of excision after OCT was performed. Specimens were removed after 24 to 48 hours from formalin, and tissue trimming was performed at the discretion of a board-certified pathologist (J.S.). Two tissue sections were collected from each artifact, and glass slides were generated for each specimen and stained with hematoxylin and eosin. Histopathology was used as a gold standard to confirm the presence of surgical artifacts and to compare histological architecture with OCT images. A histopathological assessment was made for each specimen submitted by the same board-certified pathologist (J.S.) who was masked from the results of the OCT. Slides were digitized in digital pathology software (NDP.view2 Nanozoomer; Hamatsu Photonics, Hamatsu City, Japan), viewed at ×4, and oriented on the basis of OCT images.
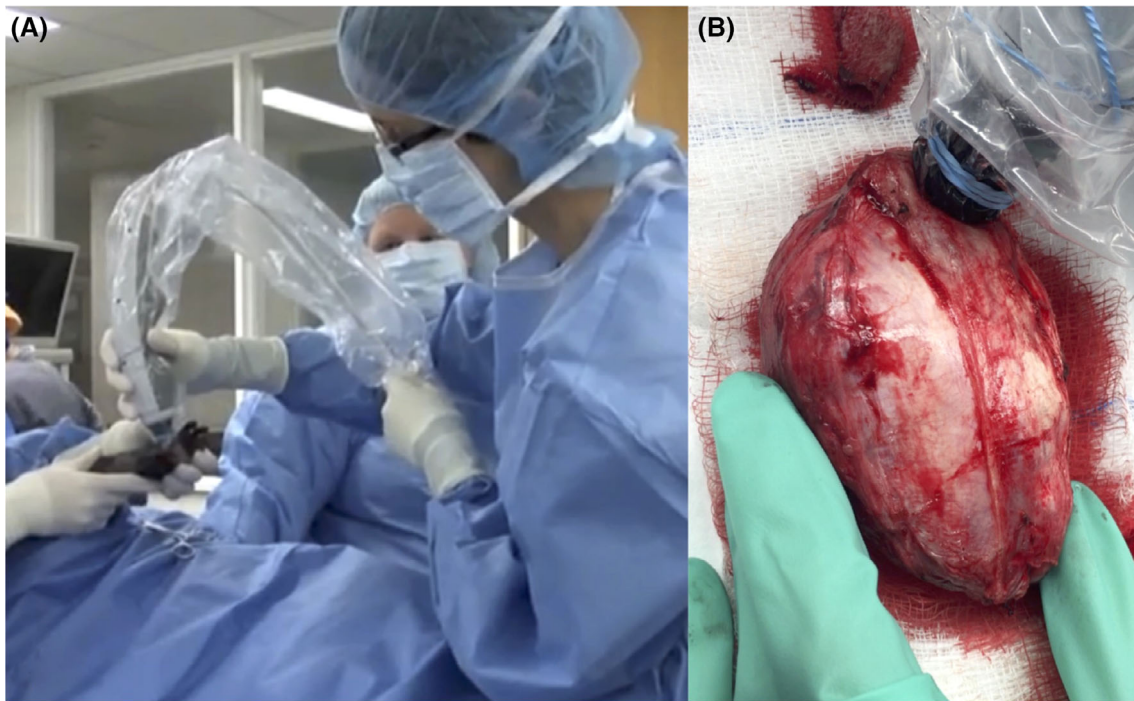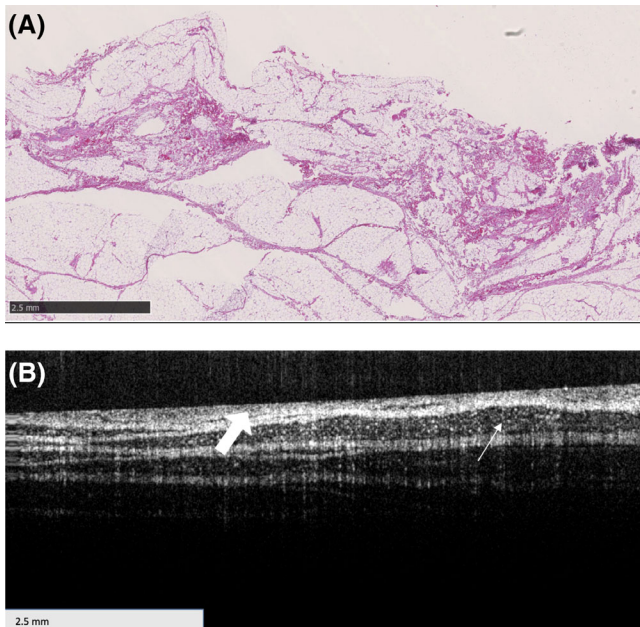

FIGURE 1 Photographs illustrating the use of a spectral domain OCT system for in vivo and ex vivo tissue analysis. A, Handheld OCT probe is used intraoperatively to evaluate a resection bed after digit amputation. B, OCT probe is held in light contact with the tissue surface and systematically swept along the lateral and deep margins of an excised tissue specimen for image acquisition. OCT, optical coherence tomography

2.5 | Comparisons

Static OCT images were directly compared to histopathology at a similar magnification by a board-certified surgeon (L.E.S.) masked to the results of artifact induction. A training set was created consisting of histopathology slides, with a known pathologic interpretation and knowledge of surgical artifact induction, paired with their respective OCT images. This created a small library of images in which the histopathological appearance of surgical artifacts could be exemplified and directly related to their OCT counterparts. The normal and abnormal features identified on OCT were compared to each specimen's histopathological counterpart by the same board-certified surgeon (L.E.S.), and trends observed among the different tissue types were noted. The results of this training set were used in subsequent evaluations to document similarities and differences of the OCT appearance of surgical artifacts among and between different tissue types.

3 | RESULTS

Results of OCT of surgical artifacts within skin samples were highly inconsistent among repeated trials. The irregular nature of the tissue after surgical artifact creation likely contributed to poor tissue-to-probe contact. These samples were not included in the training set as a result.

3.1 | Blood pooling artifact

Blood pooling artifacts created on adipose tissue, skeletal muscle, and fascia did not yield any histopathological abnormalities as a result of blood being lost during tissue processing. Optical coherence tomographic images of blood pooling artifacts revealed the presence of an area of high or increased scattering on the tissue surface (Figures 2B, 3B, 4B). The normal architecture of adipose tissue, skeletal muscle, and fascia was retained in each case beneath the blood artifact.

3.2 | Crushing artifact

Crushing artifacts created within two of three tissue types were not readily identified by histopathology. Adipose tissue was the only tissue type to show a focal area of depression consistent with a crushing artifact. Optical coherence tomographic images of crushing artifacts within adipose tissue appeared as numerous areas of condensed, high-scattering regions secondary to physical compression of the tissue. Crushing injury induced in skeletal muscle and fascial samples created physical distortion of the tissue, resulting in a serrated appearance. This created decreased probe-tissue contact and trapped air pockets represented as focal, low-scattering regions (Figures 5B and 6B). The areas of
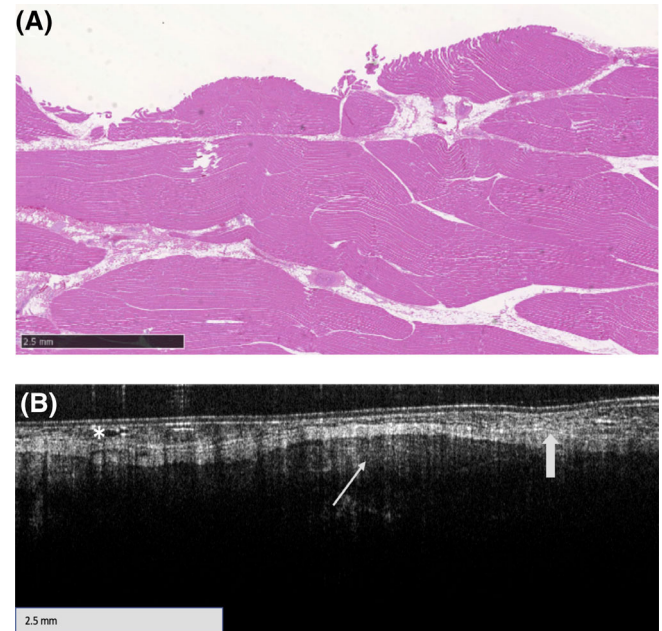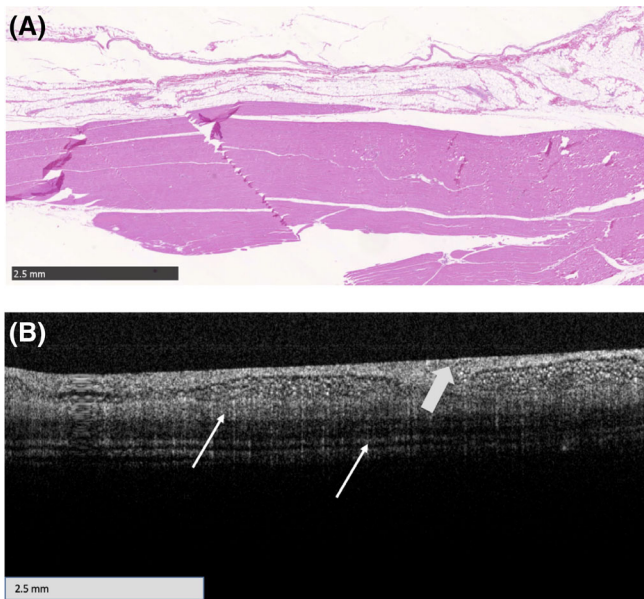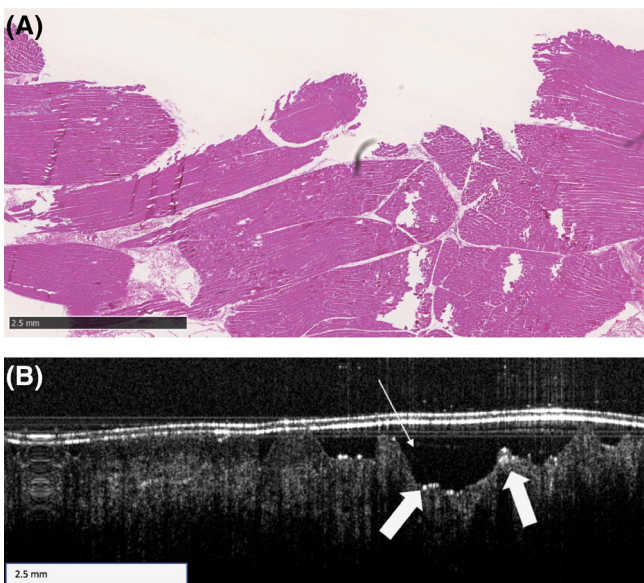

FIGURE 2 Blood pooling artifact on adipose tissue. Histopathology with hematoxylin and eosin stain (A) and OCT image (B). No histopathologic abnormalities are visible. Normal adipose tissue appears as vacuolated and honeycomb in appearance (thin white arrow, B) with OCT imaging. The area of increased scatter on the tissue surface (thick white arrow, B) represents blood pooling artifact. OCT, optical coherence tomography
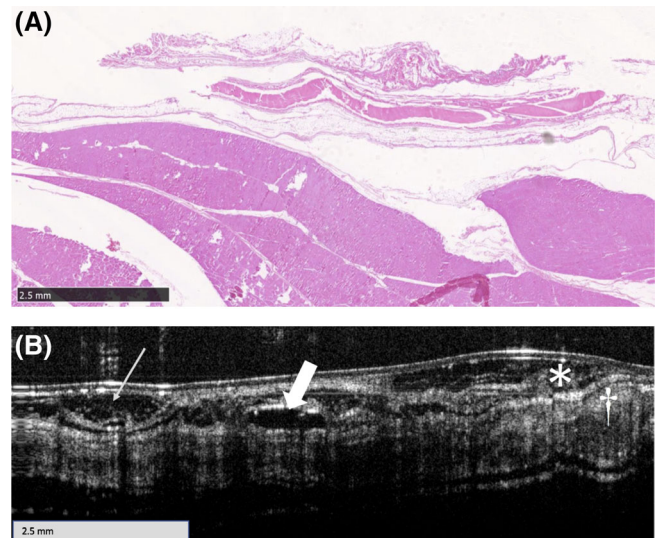

FIGURE 3 Blood pooling artifact on skeletal muscle. Histopathology with hematoxylin and eosin stain (A) and OCT image (B). No histopathologic abnormalities are visible. OCT image exhibits the normal, homogenous architecture of skeletal muscle (thin white arrow, B). A high-scatter region (thick white arrow, B) on the surface of the skeletal muscle represents blood pooling. Small, focal low-scatter regions (asterisk, B) represent the uneven surface of skeletal muscle and resultant air pockets. OCT, optical coherence tomography

FIGURE 4 Blood pooling artifact on fascial tissue. Histopathology with hematoxylin and eosin stain (A) and OCT image (B). No histopathologic abnormalities are visible. A high-scattering layer on the superficial aspect of the fascia (thick white arrow, B) represents blood pooling artifact. Interspersed within this area is the normal architecture of the fascia (thin white arrows, B). OCT, optical coherence tomography

FIGURE 5 Crushing artifact on skeletal muscle. Histopathology with hematoxylin and eosin stain (A) and OCT image (B). No histopathologic abnormalities are visible. OCT image reveals multiple, focal, low-scatter regions (thin white arrow, B) that represent air pockets from poor tissue contact. Smaller, punctate, high-scatter regions (thick white arrows, B) within this area resulted from crushing and compression of the tissue. OCT, optical coherence tomography

FIGURE 6 Crushing artifact on fascia. Histopathology with hematoxylin and eosin stain (A) and OCT image (B). No histopathologic abnormalities are visible. OCT image reveals interspersed adipose tissue (thin white arrow, B) and trapped air pockets (thick white arrow, B) overlying the fascial tissue (dagger, B). The crushing artifact has changed the conformation of the tissue, creating a serrated appearance and high-scatter region (asterisk, B) on the most superficial aspect of the fascia. OCT, optical coherence tomography

condensed tissue from the serrated conformation appear as punctate, high-scattering points (Figure 5B) or more diffuse, undulating high-scattering regions (Figure 6B).
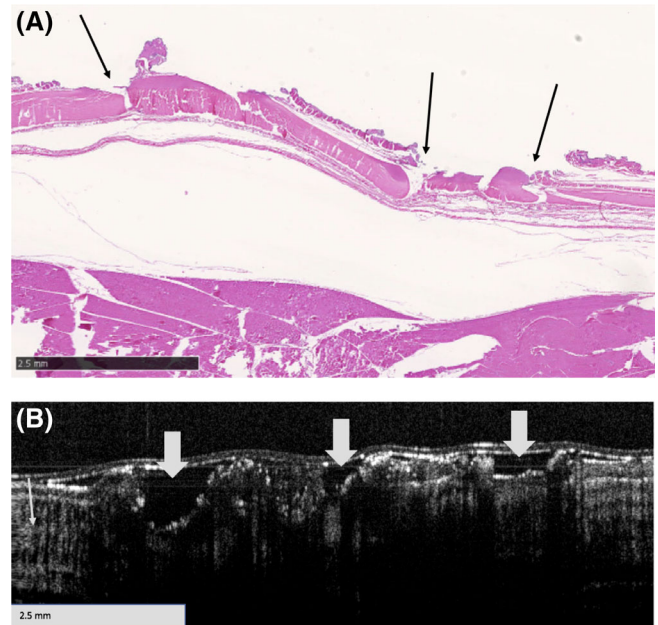
3.3 | Scalpel blade artifact

Histopathological analysis of scalpel blade artifacts did not provide evidence of significant abnormalities in any tissue type examined. Optical coherence tomographic images of scalpel blade artifacts did not identify abnormalities in two of the three tissue types evaluated. This may have been the result of changes in tissue conformation during processing. Fascia samples showed clear evidence only of a focal, low-scattering area that represented an obvious sharp cut within the tissue (Figure 7B). This area is a consequence of decreased contact between the probe-tissue interface.

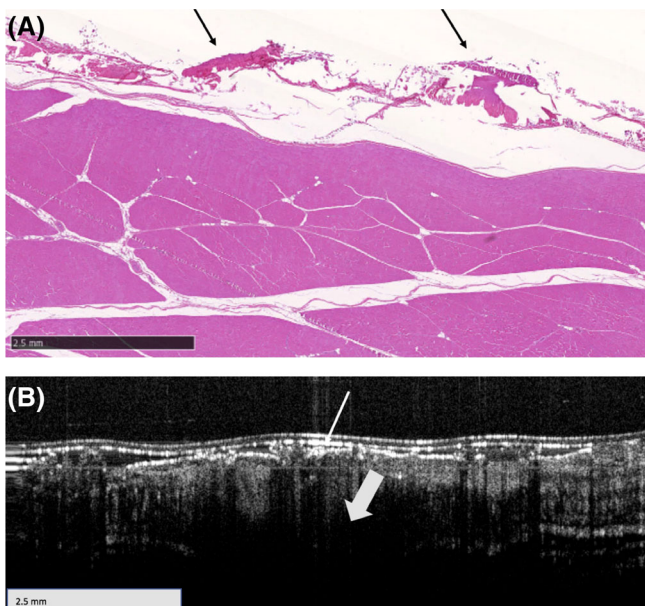## 3.4 | Monopolar electrosurgery artifact (5 W, 15 W, 25 W)

The increasing strengths of monopolar electrosurgery artifacts created a progressive increase in the severity of necrosis seen on histopathology. Necrosis was identified as the presence of homogenous eosinophilic material in adipose tissue, degenerate myocytes with hypereosinophilic and vacuolated cytoplasm in skeletal muscle, and expanded or
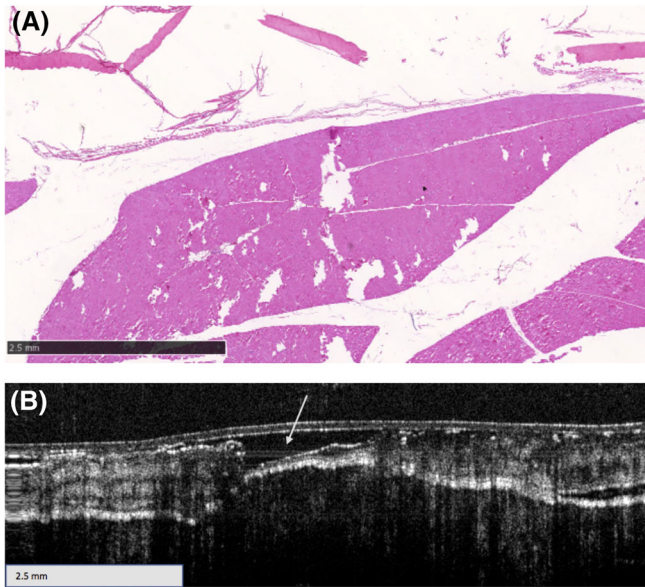
FIGURE 7 Scalpel blade artifact on fascia. Histopathology with hematoxylin and eosin stain (A) and OCT image (B). No histopathologic abnormalities are visible. OCT image reveals a focal, low-scatter area (arrow, B) that represents the scalpel blade cut. The architecture of the fascia is normal (left and right sides of image), reflecting a lack of disruption to surrounding tissues. The area of low scatter is a consequence of decreased contact between the probe-tissue interface and reflects the scalpel blade defect that has been created. OCT, optical coherence tomography

FIGURE 8 Monopolar electrosurgery (5 W) artifact on fascia. Histopathology with hematoxylin and eosin stain (A) and OCT image (B). Histopathology identifies areas of fascia that are expanded, fragmented, and filled with necrotic material (black arrows, A). The OCT image is composed of a very high-scattering layer (thin white arrow, B) on the surface of the fascia consistent with thermally induced injury. This leads to extremely superficial light penetration and lack of visualization of the underlying tissues (thick white arrow, B). OCT, optical coherence tomography

FIGURE 9 Monopolar electrosurgery (15 W) artifact on fascia. Histopathology with hematoxylin and eosin stain (A) and OCT image (B). Histopathology identifies areas of fascia that are expanded, fragmented, and filled with necrotic material (black arrows, A). The OCT (B) image illustrates a transition from normal fascia (thin white arrow) to an area of abnormal, thermal injury (thick white arrows). Normal fascia contains linear stratifications, whereas the artifact has thin, high-scatter striations present at the fascia surface (thick white arrows). Beneath this, there is a lack of penetration of light waves to deeper tissues. The focal, low-scatter regions present just beneath the thick white arrows represent trapped air pockets from an irregular tissue surface. OCT, optical coherence tomography

fragmented connective tissue filled with eosinophilic material in fascia (Figures 8–10). The depth of necrosis extended from 0.5 to 1.0 mm from the tissue surface in adipose tissue, skeletal muscle, and fascia.

Optical coherence tomographic images of adipose tissue with monopolar electrosurgery artifacts appeared as subtle, high-scattering regions with some penetration of light waves to deeper tissues at low-energy (5 W) settings (Figure 11). This progressed to pronounced and distinct high-scattering regions with a lack of visualization of deeper tissues and obvious zone of transition from normal to abnormal with higher energy settings (15 W; Figure 12).

Skeletal muscle tissue was similar to adipose tissue as increasing energy settings of monopolar electrosurgery created more exaggerated artifacts. Abnormal regions of skeletal muscle appeared as high-scattering areas with an increasing lack of depth penetration related to the power setting. Skeletal muscle also exhibited a zone of transition from normal, linear, and stratified myocytes to abnormal, disrupted regions of high-scattering tissue (Figure 13). The irregular surface of skeletal muscle after artifact induction once again created
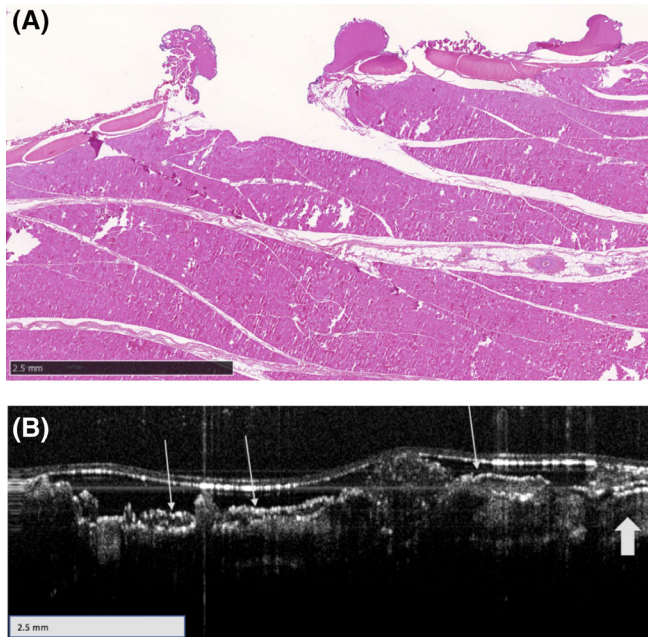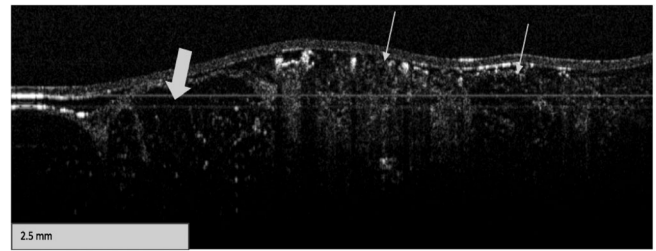
FIGURE 10 Monopolar electrosurgery (25 W) artifact on fascia. Histopathology with hematoxylin and eosin stain (A) and OCT image (B). Histopathology identifies areas of fascia that are necrotic material. The OCT image reveals a focal, high-scatter line (thin white arrows, B) present at the surface of the fascia beneath which there is poor visualization of the underlying tissue. Small amounts of normal fascia at the periphery have retained their normal structural characteristics (thick white arrow, B). OCT, optical coherence tomography
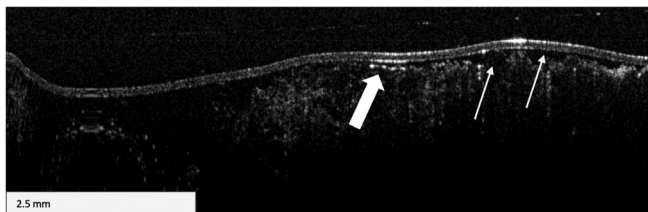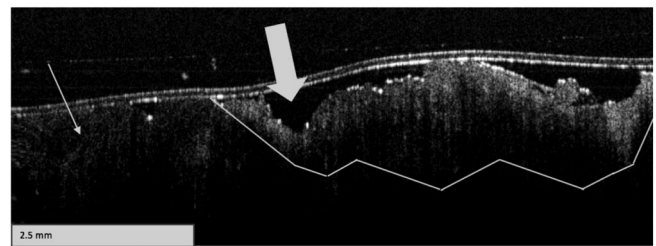

FIGURE 11 Optical coherence tomographic image of monopolar electrosurgery (5 W) artifact on adipose tissue. Thermal injury is created in the superficial connective tissue with adjacent high-scatter regions (thick white arrow) and comparatively low-scatter regions (thin white arrows) that represent air pockets or tissue irregularity. Note the ability to visualize adipose tissue beneath the areas of thermal injury

focal low-scattering regions interpreted as trapped air or fluid (Figure 13).

Optical coherence tomographic images of fascia with monopolar electrosurgery artifacts provided evidence of a highly scattering, linear region present on the surface of the tissue with a loss of the underlying linear and organized microstructural pattern of tissue. This led to extremely superficial light penetration and a lack of visualization of the underlying tissues (Figure 8B). A progressive increase in the power settings (15 W, 25 W) created irregularities in the

FIGURE 12 Optical coherence tomographic image of monopolar electrosurgery (15 W) artifact on adipose tissue. There is a zone of transition between normal adipose tissue (thick white arrow) and abnormal adipose tissue secondary to thermal injury (thin white arrows). The normal adipose tissue has a homogenous honeycomb appearance. The abnormal adipose tissue contains areas of high scatter, with some retention of its normal vacuolated appearance


FIGURE 13 Optical coherence tomographic image of monopolar electrosurgery (5 W) artifact on skeletal muscle. This image illustrates the transition between the normal and organized appearance of skeletal muscle (thin white arrow) progressing to an area of abnormal thermal injury induced by monopolar electrosurgery (white outlined area). The area of injury consists of a high-scattering and disrupted tissue surface preventing light from penetrating deeper within the skeletal muscle. Note the presence of focal, low-scatter regions (air or fluid pockets) on the irregular tissue surface (thick white arrow)

tissue surface represented as focal, low-scattering regions (Figures 8B and 9B). All samples contain a peripheral zone of normal fascia with retained cellular characteristics that transition to abnormal, high-scattering linear regions at the tissue surface (Figures 8B, 9B, 10B). This created a lack of light penetration to deeper underlying tissues and thus caused attenuation of detail of deeper tissues.

3.5 | Bipolar vessel sealing device artifact

Histopathological analysis of bipolar vessel sealing device artifacts provided evidence of abnormalities in two of the three tissue types examined. Skeletal muscle contained focal areas of degeneration with a characteristic loss of striations of myocytes (Figure 14B; top). Fascia samples contained expanded and fragmented areas of tissue filled with an eosinophilic material consistent with necrosis (Figure 14C;
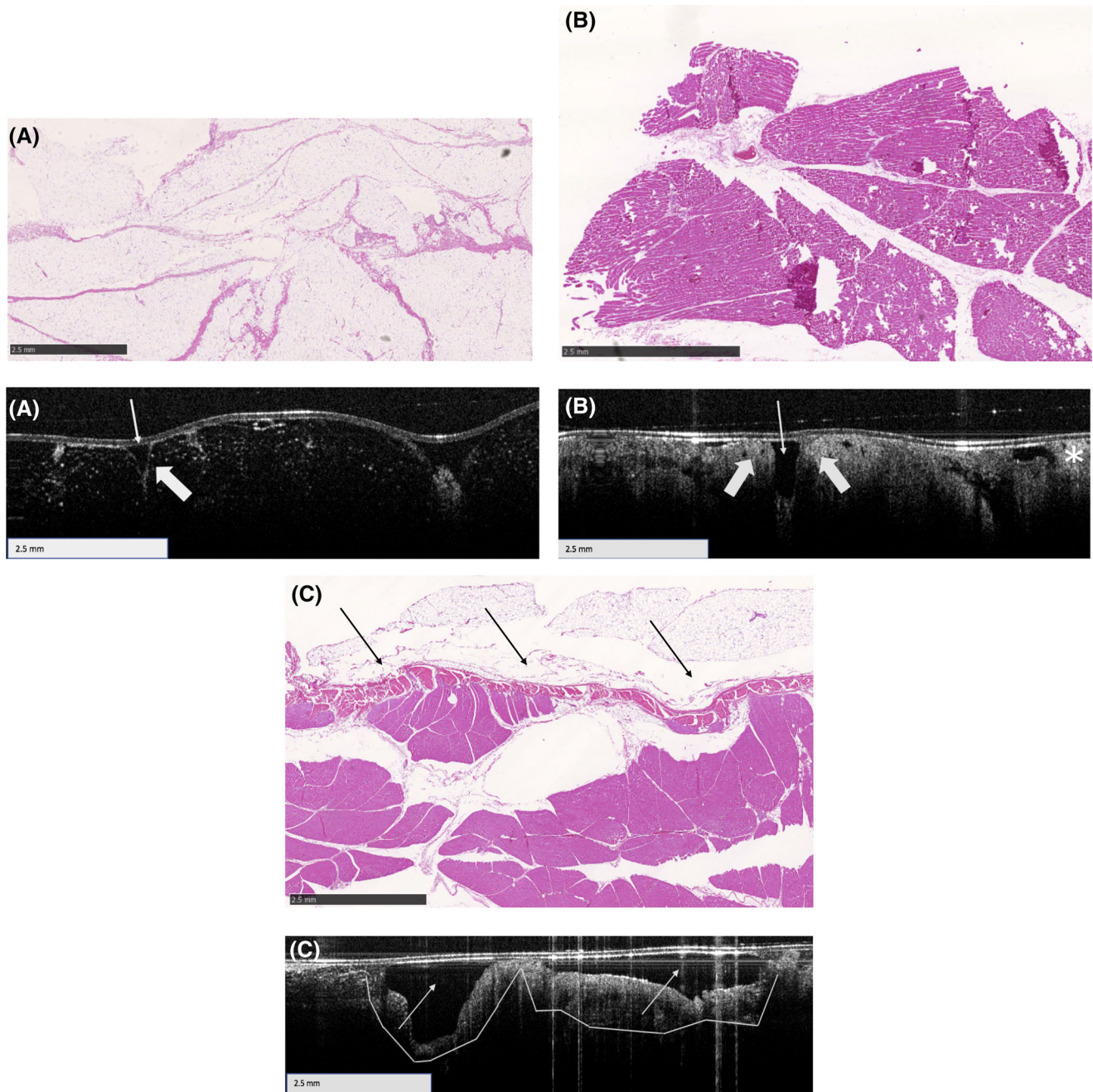
FIGURE 14 LigaSure artifacts on adipose (A), skeletal muscle (B), and fascia (C). Histopathology (top images) with hematoxylin and eosin stain and OCT images (bottom images). Histopathology of skeletal muscle (B, top) contained focal areas of degeneration with characteristic loss of striations of myocytes. Histopathology of fascia (C, top) contained expanded and fragmented tissue filled with necrotic material (black arrows). Each OCT image (A,B,C bottom) contains a focal, low-scattering cleft (thin white arrows) outlined by a high-scatter layer (thick white arrows in A and B, outlined area in C) representing the cutting and sealing functions of the device, respectively. The irregular surface of the tissue has also created pinpoint, low-scatter regions (B, bottom, asterisk) representing air pockets. OCT, optical coherence tomography

top). Optical coherence tomographic images of all bipolar vessel sealing device artifacts created a characteristic focal, low-scattering cleft outlined by a high-scattering layer representing the cutting and sealing functions of the device (Figure 14A-C; bottom). The irregular tissue surface created pinpoint, low-scattering regions due to the presence of air pockets (Figure 14B; bottom).

3.6 | Ultrasonic energy artifact

Histopathological analysis of ultrasonic energy artifacts created abnormalities in all tissue types examined. Adipose tissue contained a haphazard arrangement of collagen fibers with accumulation of eosinophilic material (Figure 15A). Skeletal muscle contained myocytes that were fragmented,
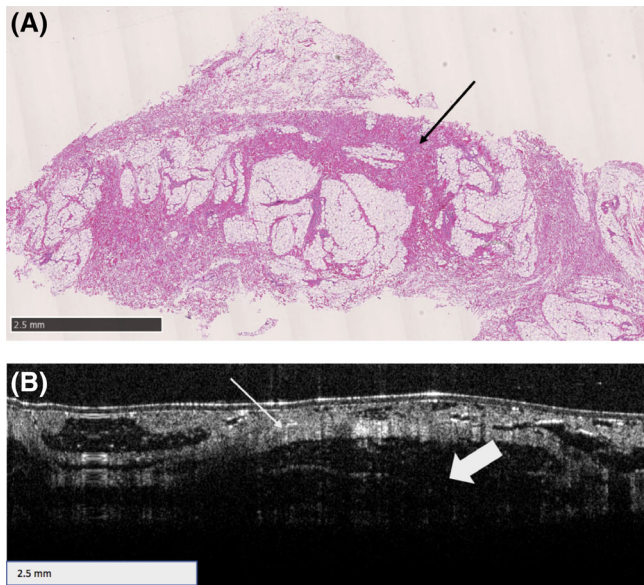
FIGURE 15 Harmonic scalpel artifact on adipose tissue. Histopathology with hematoxylin and eosin stain (A) and OCT image (B). Histopathology identifies haphazardly arranged and fragmented collagen fibers with accumulation of eosinophilic debris (black arrow, A). The adipose tissue in the OCT image (B) appears heterogenous, with a layer of high-scatter interposed with low-scattering regions (thin white arrow). This represents a layer of necrotic adipose tissue secondary to thermal injury. The layer of tissue deep to this (thick white arrow) is low-scattering and, likely, more structurally normal adipose tissue. OCT, optical coherence tomography

were hypereosinophilic, and contained pyknotic nuclei. Fascia contained areas of expansion and fragmentation that were filled with hypereosinophilic necrotic material. All histopathological abnormalities were consistent with necrosis secondary to thermal injury and extended up to 1.5 mm from the tissue surface.

Ultrasonic energy artifacts created a focal area of high-scattering regions relative to the native surrounding tissue in all OCT images evaluated. This area appeared band like and was interposed with low-scattering regions likely representing segments of normal adipose tissue (Figure 15B). The OCT appearance within skeletal muscle appeared similar, with point-like high-scattering regions that may represent individual coagulated or necrotic muscle fibers. The thermal injury represented by a high-scattering region in all cases reduced imaging penetration to deeper underlying tissue.

4 | DISCUSSION

Blood pooling, crushing, monopolar electrosurgery, bipolar vessel sealing device, and ultrasonic energy surgical artifacts created within canine tissue produced higher scattering changes and local architectural disruption to differing degrees visible on OCT images. Only the scalpel blade incision created a focal, low-scattering area representing a sharply demarcated cut within the tissue. These findings could be clinically significant because artifactual alterations created at the time of tumor excision have the potential to be misinterpreted on OCT images as incompletely resected tumor by users that do not have knowledge of the appearance of these artifacts on OCT. This misinterpretation could result in resection of additional tissue which may increase patient morbidity. Knowledge regarding the appearance of surgical artifacts can also be compiled to create an imaging library, providing insight and guidance for future OCT interpretation to increase the diagnostic accuracy of OCT for surgical margin assessment.

A generalized high-scattering appearance of artifacts was seen in most surgical instrumentation, with distinct differences observed between artifact groups. The thin, high-scattering layer overlying architecturally normal tissue observed with blood pooling was due to increased cellular density from red blood cells. Crushing artifact appeared as areas of condensed tissue with punctate or more diffuse undulating high-scattering regions. This undulating appearance was secondary to the serrated conformation of hemostatic clamps, creating physical compression of the tissue and increased density. Monopolar electrosurgery uses electromagnetic energy and resultant heat within tissue to cause protein denaturation, cell wall rupture, and tissue desiccation.[14,15] This equates to a linear increase in scattering intensity based on the power setting used and subsequent increase in tissue density. LigaSure is a bipolar vessel sealing and cutting device providing hemostasis through denaturation of collagen and elastin.[14] Optical coherence tomography revealed a focal, low-scattering region outlined by a more heterogenous, high-scattering layer. The low-scattering region represents a physical separation of tissue secondary to the cutting function of the device. The high-scattering layer represents the sealing function and is due to increased tissue density from collagen and elastin denaturation. The harmonic scalpel relies on high frequency ultrasonic waves to create vibration-induced tissue desiccation and oxidation.[14] Optical coherence tomography revealed band-like or point-like regions of high-scattering representing individual areas of coagulation or necrosis. These areas were highly scattering due to increased tissue density and subsequent amplification in backscattering of light waves. Only the scalpel blade was represented by a distinct, focal area of low-scattering intensity in contrast to these high-scattering artifacts. Two of the three tissue types examined did not identify this abnormality as a consequence of physical compression of the incision during image acquisition, creating the appearance of a solid piece of tissue.

Results of the present study are in line with previous limited descriptions of the OCT appearance of surface blood and cauterized tissue as contiguous, high-scattering areas.[7] This study however evaluated only a small subset of surgical artifacts and variability between samples and tissue types

were not assessed. Investigators in another study found that many false positive three-dimensional OCT results had corresponding histological evidence of a crushing artifact, mimicking the bright white OCT signal intensity of metastatic cell infiltration.[15] A documented description of the OCT appearance of surgical artifacts is therefore crucial to expand the imaging repertoire of observers, increase the diagnostic accuracy of surgical margin assessment, and minimize the morbidity associated with the requirement for additional and potentially unrequired surgical procedures.

Despite the superficial association that can be drawn between artifact and residual neoplastic disease, fundamental features also distinguish one from the other. In a recently published report of a study in which histological features of surgical margins from excised canine soft tissue sarcomas with OCT imaging were evaluated, Selmic et al[16] concluded that incomplete margins appeared highly dense and diffusely high scattering throughout tissue boundaries. The alignment and organization of normal tissue microstructure was absent, implying effacement with invasive neoplastic disease.[16] Surgical artifacts from this study created a focal and highly scattering char line at the superficial aspect of the tissue specimen in contrast. The surrounding tissue ultrastructure was preserved, and an abrupt zone of transition was clearly evident unlike that seen in neoplastic disease. Furthermore, despite the likelihood that there is a distinct difference between the OCT appearance of surgical artifacts and residual neoplastic disease, we cannot directly conclude this from this study because they were not directly compared. Tissue depth is another parameter that can be considered to determine whether observed changes are inherent to the natural tissue architecture. Nguyen et al[7] showed that the presence of highly scattering regions deep in the tissue margin, instead of localized to the immediate surface, increased the likelihood that these features were intrinsic to the tissue architecture rather than a result of the surgical procedure. Results of this study provided evidence that monopolar electrosurgery and ultrasonic energy artifacts created abnormalities extending anywhere from 0.5 to 1.5 mm beyond the immediate tissue surface. The depth to which surgical artifacts penetrate, however, is not only a predictor of whether the disease process is native to the tissue but also a function of the amount of energy and time with which it is applied.

The current study is not without limitations. The cadaveric nature of the study can affect OCT image resolution and contrast due to a lack of normal tissue perfusion. After artifacts were excised and submitted for histopathological analysis, shrinkage may have also caused an over- or underestimation in tissue thickness. This could have altered the appearance of artifacts and the depth to which they extended when examined with histopathology. The lack of a negative control samples could be considered a limitation; however, the OCT appearance of normal tissues were not assessed.

encountered at surgical margins in dogs after resection of soft tissue sarcomas has been previously described,[16] and the board-certified surgeon who performed all comparisons of OCT and histopathology has years of experience with OCT tissue imaging. Finally, histopathology did not always identify the presence of surgical artifacts despite samples being taken directly from OCT-imaged areas. This may have been due to imperfections associated with histological sectioning or creation of an artifact too mild to cause significant tissue abnormalities.

In conclusion, common surgical instruments and conditions encountered during tumor excision produced high-scattering OCT artifacts in tissues frequently evaluated at surgical margins in this ex vivo study. Specifically, OCT artifacts consisted of an increase in scattering intensity and disorganization within the local tissue architecture. Defining and describing the characteristics of these surgical artifacts will aid in future diagnostic OCT interpretation by eliminating false positive diagnoses and advancing the utility of OCT as a novel intraoperative imaging modality for surgical margin assessment.

CONFLICT OF INTEREST

The authors declare no conflicts of interest related to this report.

ORCID

Laura E. Selmic https://orcid.org/0000-0001-6695-6273

REFERENCES

1. Sarin R, Somsekhar S, Kumar R, et al. Practical consensus recommendations for tumor margins and breast conservative surgery. *South Asian J Cancer.* 2018;7(2):72.
2. Giudice C, Stefanello D, Sala M, et al. Feline injection-site sarcoma: recurrence, tumour grading and surgical margin status evaluated using the three-dimensional histological technique. *Vet J.* 2010;186(1):84-88.
3. Poirier VJ, Thamm DH, Kurzman ID, et al. Liposome-encapsulated doxorubicin (Doxil) and doxorubicin in the treatment of vaccine-associated sarcoma in cats. *J Vet Intern Med.* 2002;16(6):726-731.
4. John ERS, Al-khudairi R, Ashrafian H, et al. Diagnostic accuracy of intraoperative techniques for margin assessment in breast cancer surgery: a meta-analysis. *Ann Surg.* 2017;265(2):300-310.
5. Kennedy BF, McLaughlin RA, Kennedy KM, et al. Investigation of optical coherence microelastography as a method to visualize cancers in human breast tissue. *Cancer Res.* 2015;75(16):3236-3245.
6. Cabon Q, Sayag D, Texier I, et al. Evaluation of intraoperative fluorescence imaging-guided surgery in cancer-bearing dogs: a prospective proof-of-concept phase II study in 9 cases. *Transl Res.* 2016;170:73-88.
7. Nguyen FT, Zysk AM, Chaney EJ, et al. Intraoperative evaluation of breast tumor margins with optical coherence tomography. *Cancer Res.* 2009;69(22):8790-8796.

8. Boppart SA, Bouma BE, Pitris C, Southern JF, Brezinski ME, Fujimoto JG. In vivo cellular optical coherence tomography imaging. *Nat Med.* 1998;4(7):861-865.

9. Boppart SA, Deutsch TF, Rattner DW. Optical imaging technology in minimally invasive surgery. Current status and future directions. *Surg Endosc.* 1999;13(7):718-722.

10. Fujimoto JG, Pitris C, Boppart SA, Brezinski ME. Optical coherence tomography: an emerging technology for biomedical imaging and optical biopsy. *Neoplasia.* 2000;2(1–2):9-25.

11. Huang D, Swanson EA, Lin CP, et al. Optical coherence tomography. *Science.* 1991;254(5035):1178-1181.

12. Mesa KJ, Selmic LE, Pande P, et al. Intraoperative optical coherence tomography for soft tissue sarcoma differentiation and margin identification. *Lasers Surg Med.* 2017;49(3):240-248.

13. Cocca C. Use of optical coherence tomography for directed pathological sectioning of surgical margins of resected tumors. Presented at: Veterinary Society of Surgical Oncology 2018 Symposium; April 9–11, 2018; Maui, Hawaii.

14. Tobias KM, Johnston SA. Principles and use of energy sources in small animal surgery: electrosurgery and laser applications. In: Tobias KM, Johnston SA, eds. *Veterinary Surgery: Small Animal.* Vol 1. 2nd ed. St Louis, MO: Elsevier; 2018:200-206.

15. Nolan RM, Adie SG, Marjanovic M, et al. Intraoperative optical coherence tomography for assessing human lymph nodes for metastatic cancer. *BMC Cancer.* 2016;16:144.

16. Selmic LE, Samuelson J, Reagan JK, et al. Intra-operative imaging of surgical margins of canine soft tissue sarcoma using optical coherence tomography. *Veterinary and Comparative Oncology.* 2019;17(1):80-88.